Inorganic Chemistry

Communication

pubs.acs.org/IC

Application of the Rotating Ring-Disc-Electrode Technique to Water Oxidation by Surface-Bound Molecular Catalysts

Javier J. Concepcion, Robert A. Binstead, Leila Alibabaei, and Thomas J. Meyer*

Department of Chemistry, University of North Carolina at Chapel Hill, Chapel Hill, North Carolina 27514, United States

Supporting Information

ABSTRACT: We report here the application of a simple hydrodynamic technique, linear sweep voltammetry with a modified rotating-ring-disc electrode, for the study of water oxidation catalysis. With this technique, we have been able to reliably obtain turnover frequencies, overpotentials, Faradaic conversion efficiencies, and mechanistic information from single samples of surface-bound metal complex catalysts.

Water oxidation, $2H_2O \rightarrow O_2 + 4H^+ + 4e^-$, is the fundamental "other half-reaction" in energy conversion processes in plant photosynthesis and in solar fuel applications in artificial photosynthesis.[1−3] The first designed molecular catalyst for water oxidation was the "ruthenium blue dimer", *cis*,*cis*-$[(bpy)_2(OH_2)Ru^{III}ORu^{III}(bpy)_2(OH_2)]^{4+}$.[4] Interest in this area has blossomed with multiple single-site water oxidation catalysts reported, mainly based on $Ru^V{=}O$ and $Ir^V{=}O$ intermediates.[5−9]

In investigating water oxidation mechanism and catalysis by molecular complexes, the most commonly used oxidants have been salts of cerium(IV).[5,6,8,10−15] These reagents are limited to strongly acidic solutions, pH ≤ 1, because of hydrolysis and loss of the oxidative driving force. Electrochemical techniques offer a much wider latitude in solution conditions with additional mechanistic insight available by surface binding to electrode surfaces.[16,17]

Recently, Murray et al. applied rotating-disc-electrode (RDE) and rotating-ring-disc-electrode (RRDE) techniques to study water oxidation electrocatalysis by iridium dioxide nanoparticles.[18,19] A key element in these experiments was attachment of the nanoparticles to the disc. Analysis of RRDE data for solution catalysts is complicated, especially when the substrate is the solvent. At the potentials used for oxygen detection at the ring, competitive reduction of the oxidized catalyst also occurs.

We report here the application of RRDE techniques to the study of water oxidation catalysis by surface-confined ruthenium(II) polypyridyl molecular catalysts. We show that this technique offers unprecedented insight with a single set of experiments providing turnover frequencies as a function of the overpotential, the onset potential for water oxidation, and quantitative product analysis at the ring. The technique is based on anchoring catalysts to glassy carbon disc electrodes that are surface-modified by the addition of tin-doped indium oxide (ITO); see Supporting Information (SI) for details. The presence of the particles on the disc is easily identified by an increase in the capacitive current during cyclic voltammetry scans compared to unmodified electrodes (Figure 2) and by scanning electron microscopy (Figure S2 in the SI). Once the glassy carbon electrode has been modified with the metal oxide nanoparticles, the catalyst is loaded onto the nanoparticles by using standard anchoring groups [−COOH, $-PO(OH)_2$, etc.]. In this work, we compare the performance of two known ruthenium-based, single-site water oxidation catalysts (Figure 1) with respect to overpotentials, turnover frequencies, and Faradaic conversion efficiencies for water oxidation.

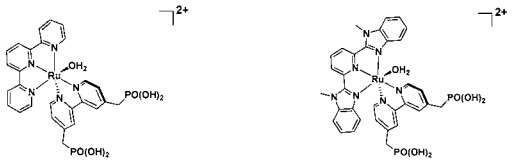

1 2

Figure 1. Structures of **1** and **2**.

Figure 2 shows a cyclic voltammogram of $[Ru^{II}(Mebimpy)(4,4'\text{-}(PO(OH)_2\text{-}CH_2)_2\text{-}bpy)(OH_2)]^{2+}$ (**2**, Figure 1) on a nano-

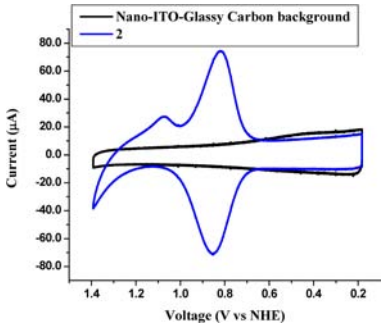

Figure 2. Blue: Cyclic voltammogram of **2** on nano-ITO−glassy carbon in 0.1 M $HClO_4$. Scan rate: 100 mV/s (see the text for details).

ITO-RRDE in 0.1 M $HClO_4$. A background scan is also shown under the same conditions. Similar data for $[Ru^{II}(tpy)(4,4'\text{-}(PO(OH)_2\text{-}CH_2)_2\text{-}bpy)(OH_2)]^{2+}$ (**1**, Figure 1) are shown in Figure S4 in the SI. A prominent surface wave for the surface-bound $-Ru^{III}OH_2^{3+}/-Ru^{II}OH_2^{2+}$ couple of **2** is observed with a separation of 35 mV between the anodic and cathodic peak potentials. This is indicative of good conductivity and homogeneity throughout the nano-ITO film. The $-Ru^{IV}{=}$

Received: September 2, 2013
Published: September 19, 2013

   dx.doi.org/10.1021/ic402240t | *Inorg. Chem.* 2013, 52, 10744−10746

$O^{2+}/-Ru^{III}OH_2^{3+}$ couple is well separated from the $-Ru^{III}OH_2^{3+}/-Ru^{II}OH_2^{2+}$ couple, but it is kinetically more inhibited than that for **1**.[20] A partial reduction wave for this couple is observed at 1.05 V. Integration of the $Ru^{III}OH_2^{3+}/Ru^{II}OH_2^{2+}$ wave gives a surface coverage (Γ) of 6.4×10^{-9} mol/cm^2 over the projected area of the 0.196 cm^2 glassy carbon disc, which is the equivalent of ~64 electroactive monolayers on a planar surface.[21] For **1**, $\Gamma = 5.8 \times 10^{-9}$ mol/cm^2 was found, the equivalent of ~58 electroactive monolayers. No attempt was made to quantify the per particle catalyst loading.

A second experiment was conducted with **2** attached to the nano-ITO disc. The blue trace displays this result with the potential scanned at 10 mV/s from 1.00 to 1.79 V. A wave corresponding to the oxidation of $-Ru^{III}OH_2^{3+}$ to $-Ru^{IV}{=}O^{2+}$ is clearly observed, followed by a steep increase in the current starting at ~1.45 V. The wave for the oxidation of $-Ru^{II}OH_2^{2+}$ to $-Ru^{III}OH_2^{3+}$ appears below 1.0 V. The red trace shows the corresponding reductive current at the platinum ring, which begins to increase at ~1.49 V. This is expected because of the generation of oxygen at the disc and reduction to H_2O at the ring (as determined with a platinum disc–platinum ring RRDE; see the SI). Generation of oxygen at the disc begins to occur 320 mV above the thermodynamic potential for water oxidation at pH 1 (1.17 V). Similar experiments for **1** are shown in Figure S5 in the SI. The onset potential for water oxidation by **2** is 115 mV lower than that for **1**.

For linear sweep voltammetry (LSV) at a RDE, the current at the disc is given by the Koutecký–Levich equation, eq 1 (see the SI for explanation of terms).[22] For water oxidation in aqueous solutions, water is the substrate, and because the catalysts are surface-immobilized, the limiting current in RDE experiments is independent of the rotation and scan rates.

$$\frac{1}{i} = \frac{1}{i_K} + \frac{1}{0.62nFAD_0^{2/3}\omega^{1/2}\nu^{-1/6}C_0^*} \quad (1)$$

Thus, the catalytic current for water oxidation in these experiments is dictated by the turnover frequency of the catalyst at the applied potential E [$k_{cat}(E)$], the surface loading of the catalyst (Γ), and the area of the electrode (A), eq 2.[23]

$$i_{cat} = nFA\Gamma k_{cat}(E) \quad (2)$$

Turnover frequencies, as $k_{cat}(E)$, as a function of the applied potential for **2** in 0.1 M $HClO_4$ are shown in Figure S6 in the SI and for **1** in Figure S7 in the SI. They were determined by use of eq 2. The blue trace shows the values obtained by assuming that all the oxidative current results in water oxidation to oxygen at the disc. It reaches $k_{cat}(E) = 0.18$ s^{-1} at 1.65 V and remains constant to 1.79 V. This is 3 times faster than the rate observed for **1** at the same potential. The red trace shows the values obtained from the actual evolved oxygen measured at the ring. These data have been corrected for background current in the absence of **2**. It has also been corrected (×4.0) for the collection efficiency (24.9%) of the ring electrode, which is dictated by the ring-disc geometry; see the SI. It reaches a maximum of 0.09 s^{-1} at 1.79 V, 50% of the value calculated from the oxidative current. *No hydrogen peroxide was detected by holding the potential of the ring at 1.13 V, where the oxidation of hydrogen peroxide to oxygen at platinum is diffusion-limited; see Figures S11–S13 in the SI.*

For both catalysts, the turnover frequency as a function of the applied potential displays two regimes. Initially, it increases as the applied potential is increased. This is because the concentration of the catalytically active form, $Ru^V{=}O^{3+}$, increases according to the Nernst equation as the applied potential approaches $E_{1/2}$ for the $Ru^V{=}O^{3+}/Ru^{IV}{=}O^{2+}$ couple. At some point, the turnover frequency is dictated by the rate of O–O bond formation and enters a second regime independent of the applied potential. The potential at which the change between the two regimes takes place is significant because it points to a change in the rate-limiting behavior in the catalytic cycle. It also provides a good estimate of $E_{1/2}$ for the apparently irreversible $Ru^V{=}O^{3+}/Ru^{IV}{=}O^{2+}$ couple.

This conclusion is further supported by Figure S3 in the SI, which shows the Faradaic efficiency (η_F) as a function of the applied potential, with η_F the fraction of the total current passed that is used to oxidize water to oxygen. It was calculated as the ratio of the ring to disc current with background and collection efficiency corrections ×100%. It varies from 0 at 1.49 V to ~50% at ~1.65 V, with a 16 mV window between the onset potential and the maximum efficiency for oxygen generation. The efficiency remains constant from 1.65 to 1.79 V.

In the RRDE experiment, the turnover frequency, $k_{cat}(E)$, provides kinetic information about the key O---O bond-forming step in the reaction between $Ru^V(O)^{3+}$ and water in Scheme S1 to give a detectable peroxide intermediate.[5,6,16] Past the $Ru^V{=}O^{3+}/Ru^{IV}{=}O^{2+}$ couple, k_{O-O} is the turnover frequency, and $k_{cat}(E) = k_{O-O}$.

The RRDE experiment on nano-ITO provides additional insight about catalyst stability. Faradaic efficiencies for oxygen generation by catalyst **1** only reach 27%, with 73% of the anodic current not leading to oxygen production. As for **2**, there was no evidence for hydrogen peroxide production at the ring at 1.13 V, where hydrogen peroxide oxidation at platinum is diffusion-limited. The loss in the Faradaic efficiency provides direct evidence for catalyst deactivation. Additional evidence appears in the change in the i–V behavior after a series of LSV scans (Figure S14 in the SI). For catalyst **2**, the Faradaic efficiency reaches 50%, just 16 mV past its onset potential, without evidence for deactivation after multiple RRDE scans (Figure 3). Control

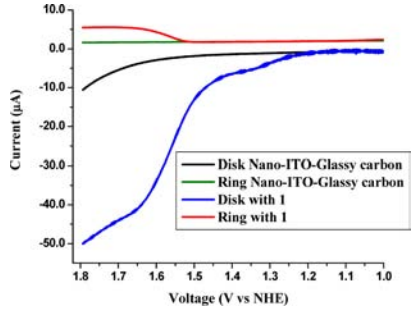

Figure 3. RRDE voltammogram in 0.1 M $HClO_4$ (see the text for details).

experiments show that the unaccounted for anodic current for **2** arises, at least in part, from oxidation of the glassy carbon electrode by the catalyst. Experiments are underway to overcome this limitation.

The advantages in applying the RRDE technique to catalytic water oxidation for surface-bound catalysts are clear. Quantitative information is provided concerning (1) rates, by measurement of the turnover frequencies, (2) the appearance of O_2 and/or H_2O_2 as products both qualitatively and quantitatively, (3) Faradaic efficiencies for O_2 production and/or H_2O_2 formation, (4) overpotentials, and (5) evidence for catalyst instability.

dx.doi.org/10.1021/ic402240t | *Inorg. Chem.* 2013, 52, 10744–10746

■ ASSOCIATED CONTENT

Supporting Information

Detailed experimental procedures. This material is available free of charge via the Internet at http://pubs.acs.org.

■ AUTHOR INFORMATION

Corresponding Author

*E-mail: tjmeyer@unc.edu.

Notes

The authors declare no competing financial interest.

■ ACKNOWLEDGMENTS

This work was partially funded by the UNC Energy Frontier Research Center (EFRC) "Center for Solar Fuels", an EFRC funded by the U.S. Department of Energy, Office of Science, Office of Basic Energy Sciences, under Award DE-SC0001011, which supported J.J.C., R.A.B., and T.J.M.. Support for L.A. and T.J.M. was provided by Research Triangle Solar Fuels Institute. We acknowledge support for the purchase of instrumentation from the UNC EFRC (Center for Solar Fuels), funded by the U.S. Department of Energy, Office of Science, Office of Basic Energy Sciences, under Award DE-SC0001011, and UNC SERC ("Solar Energy Research Center Instrumentation Facility"), funded by the U.S. Department of Energy Office of Energy Efficiency & Renewable Energy under Award DE-EE0003188.

■ REFERENCES

(1) Alstrum-Acevedo, J. H.; Brennaman, M. K.; Meyer, T. J. *Inorg. Chem.* **2005**, *44*, 6802.

(2) Gust, D.; Moore, T. A.; Moore, A. L. *Acc. Chem. Res.* **2009**, *42*, 1890.

(3) Renger, G.; Renger, T. *Photosynth. Res.* **2008**, *98*, 53.

(4) Gersten, S. W.; Samuels, G. J.; Meyer, T. J. *J. Am. Chem. Soc.* **1982**, *104*, 4029.

(5) Concepcion, J. J.; Tsai, M. K.; Muckerman, J. T.; Meyer, T. J. *J. Am. Chem. Soc.* **2010**, *132*, 1545.

(6) Concepcion, J. J.; Jurss, J. W.; Templeton, J. L.; Meyer, T. J. *J. Am. Chem. Soc.* **2008**, *130*, 16462.

(7) Blakemore, J. D.; Schley, N. D.; Balcells, D.; Hull, J. F.; Olack, G. W.; Incarvito, C. D.; Eisenstein, O.; Brudvig, G. W.; Crabtree, R. H. *J. Am. Chem. Soc.* **2010**, *132*, 16017.

(8) Hull, J. F.; Balcells, D.; Blakemore, J. D.; Incarvito, C. D.; Eisenstein, O.; Brudvig, G. W.; Crabtree, R. H. *J. Am. Chem. Soc.* **2009**, *131*, 8730.

(9) Tseng, H.-W.; Zong, R.; Muckerman, J. T.; Thummel, R. *Inorg. Chem.* **2008**, *47*, 11763.

(10) Binstead, R. A.; Chronister, C. W.; Ni, J. F.; Hartshorn, C. M.; Meyer, T. J. *J. Am. Chem. Soc.* **2000**, *122*, 8464.

(11) Bozoglian, F.; Romain, S.; Ertem, M. Z.; Todorova, T. K.; Sens, C.; Mola, J.; Rodriguez, M.; Romero, I.; Benet-Buchholz, J.; Fontrodona, X.; Cramer, C. J.; Gagliardi, L.; Llobet, A. *J. Am. Chem. Soc.* **2009**, *131*, 15176.

(12) Duan, L. B. F.; Mandal, S.; Stewart, B.; Privalov, T.; Llobet, A.; Sun, L. *Nat. Chem.* **2012**, *4*, 418.

(13) Duan, L. F. A.; Xu, Y.; Sun, L. *J. Am. Chem. Soc.* **2009**, *131*, 10397.

(14) Francas, L.; Sala, X.; Escudero-Adan, E.; Benet-Buchholz, J.; Escriche, L.; Llobet, A. *Inorg. Chem.* **2011**, *50*, 2771.

(15) Liu, F.; Concepcion, J. J.; Jurss, J. W.; Cardolaccia, T.; Templeton, J. L.; Meyer, T. J. *Inorg. Chem.* **2008**, *47*, 1727.

(16) Chen, Z. F.; Concepcion, J. J.; Jurss, J. W.; Meyer, T. J. *J. Am. Chem. Soc.* **2009**, *131*, 15580.

(17) Concepcion, J. J.; Jurss, J. W.; Hoertz, P. G.; Meyer, T. J. *Angew. Chem., Int. Ed.* **2009**, *48*, 9473.

(18) Nakagawa, T.; Beasley, C. A.; Murray, R. W. *J. Phys. Chem. C* **2009**, *113*, 12958.

(19) Nakagawa, T.; Bjorge, N. S.; Murray, R. W. *J. Am. Chem. Soc.* **2009**, *131*, 15578.

(20) Chen, Z.; Vannucci, A. K.; Concepcion, J. J.; Jurss, J. W.; Meyer, T. J. *Proc. Natl. Acad. Sci. U.S.A.* **2011**, *108*, E1461.

(21) Meyer, T. J.; Meyer, G. J.; Pfennig, B. W.; Schoonover, J. R.; Timpson, C. J.; Wall, J. F.; Kobusch, C.; Chen, X. H.; Peek, B. M.; Wall, C. G.; Ou, W.; Erickson, B. W.; Bignozzi, C. A. *Inorg. Chem.* **1994**, *33*, 3952.

(22) Bard, A. J. F.; Larry, R. *Electrochemical Methods: Fundamentals and Applications*, 2nd ed.; John Wiley & Sons, Inc.: New York, 2001.

(23) Elliott, S. J.; McElhaney, A. E.; Feng, C. J.; Enemark, J. H.; Armstrong, F. A. *J. Am. Chem. Soc.* **2002**, *124*, 11612.